High-pressure study of pyridine-mediated electrochemical reduction of CO_2 to methanol at a platinum electrode

S. I. Rybchenko, D. Touhami, J. D. Wadhawan, S. K. Haywood.

School of Engineering, University of Hull, Cottingham Road, Hull, HU6 7RX, UK

Abstract

The recently proposed highly efficient route of pyridine-catalysed CO_2 reduction to methanol was explored on platinum electrodes at high CO_2 pressure.

At 55 bars of CO_2, the bulk electrolysis in both potentiostatic and galvanostatic regimes resulted in methanol production with Faradaic yield up to 10% for the first 5-10 C/cm^2 of charge passed. For longer electrolysis, the methanol concentration failed to increase proportionally, being limited to sub-ppm levels irrespective of biasing conditions and pyridine concentration. This limitation cannot be removed by electrode reactivation and/or pre-electrolysis and appears to be an inherent feature of the reduction process.
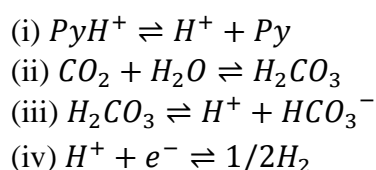
In agreement with bulk electrolysis findings, the CV analysis supported by simulation indicated that hydrogen evolution is still the dominant electrode reaction in pyridine-containing electrolyte, even at excess CO_2 concentration in the electrolyte. No prominent contribution from either a direct or coupled CO_2 reduction was found.

The results obtained suggest that the CO_2 to methanol reduction is a transient process that is largely decoupled from the electrode charge transfer.

Introduction

Recently, significant research effort has been directed towards the option of reducing captured CO_2 to fuels and high value chemicals, as an alternative approach to carbon capture and sequestration, which is costly both financially and in energy terms, requiring 10-40% of the energy produced by a coal power station.[1]. Among the most promising routes is the catalytic electrochemical and photo-electrochemical reduction of CO_2 to products such as methanol or formic acid. Electrochemical routes to both molecules are already being exploited commercially[2-4] using wind or geothermal energy. However, as the reduction of CO_2 is thermodynamically expensive, any reduction in the over-potential required or increase in Faradaic efficiency would be valuable. Similarly, increasing product selectivity to minimise the energy needed for separation and purification would also be a key improvement to the reduction process. Hence, recent reports of highly efficient and selective reduction of CO_2 to methanol in pyridine-containing aqueous electrolytes were very encouraging. Faradaic efficiencies of 100% were reported on p-GaP[5] and of ca. 20% on Pt[6] cathodes at very low overpotentials. Methanol production was suggested to proceed through a 6-electron multi-step reduction process mediated by pyridine (Py). The mechanism initially proposed[6,7] involved pyridine protonation in acidic media to pyridinium (PyH⁺), followed by charge transfer on the electrode creating a pyridinium radical. It was suggested that this pyridinium radical then interacts with CO_2 to generate an intermediate carbamate radical complex, via a multistep inner-sphere mechanism leading to the alcohol formation. The cyclic voltammetry (CV) wave representing the single-electron charge transfer in pyridine-containing electrolyte has been observed on some other electrodes such as Pd[8], p-GaP[5], Pt/C-TiO₂[9] and iron pyrites.[10] These reports stimulated several theoretical calculations related to the proposed mechanism based on the pyridinium radical. In particular, the pyridinium reduction potential has been calculated by two independent groups. Although there were discrepancies between the exact values reported by these groups, there was general agreement that the reduction of the pyridinium occurs at a potential at least 0.6V more negative than is experimentally observed in the CV of the pyridine system.[11-14] This fact has made the mechanism initially proposed improbable and stimulated further investigations.
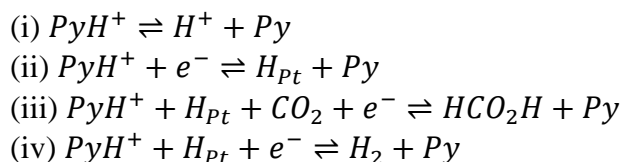
Scheme 1. Proposed mechanism of the electrochemical reduction in aqueous acidic pyridine solution on Pt electrode.

$$(i)\ PyH^+ \rightleftharpoons H^+ + Py$$
$$(ii)\ CO_2 + H_2O \rightleftharpoons H_2CO_3$$
$$(iii)\ H_2CO_3 \rightleftharpoons H^+ + HCO_3^-$$
$$(iv)\ H^+ + e^- \rightleftharpoons 1/2H_2$$

Further voltammetric studies of pyridinium ions on a Pt electrode revealed some features in common with the behaviour of weak acids.[15,16] Costentin et al. proposed that the pyridinium behaves as any weak acid undergoing reduction on a Pt electrode, leading exclusively to hydrogen generation.[15] According to these authors, the peak current observed under inert atmosphere is merely the reduction of hydrated protons diffused to the electrode surface (Scheme 1, reaction iv). The protons are released by the pyridinium acting as a weak acid via a fast deprotonation equilibrium (Scheme 1, reaction i). This group argues that the mechanism leading to the catalytic current observed under CO_2 does not differ much from the current resulting under an inert gas; the enhancement of the former being due to increased proton concentration resulting from carbonic acid dissociation (Scheme 1, reaction iii). This interpretation together with their NMR analysis of the electrolysis products, which showed no sign of methanol, allowed them to explicitly

rule out the catalytic role of pyridinium in methanol production. In subsequent/more recent papers by the Bocarsly group another mechanism of pyridine-assisted methanol synthesis was brought forward. In agreement with [13], it was suggested[17-19] that the Pt electrode surface plays a key role in the multistep CO_2 reduction to methanol. The first CO_2 reduction step is detailed in Scheme 2.

Scheme 2. Proposed mechanism of pyridine-assisted electrochemical reduction of CO_2 on Pt electrodes in aqueous acidic solution.

$$\text{(i) } PyH^+ \rightleftharpoons H^+ + Py$$
$$\text{(ii) } PyH^+ + e^- \rightleftharpoons H_{Pt} + Py$$
$$\text{(iii) } PyH^+ + H_{Pt} + CO_2 + e^- \rightleftharpoons HCO_2H + Py$$
$$\text{(iv) } PyH^+ + H_{Pt} + e^- \rightleftharpoons H_2 + Py$$

In contrast to Scheme 1, in this scheme 5-25% of the reduction current was estimated to be responsible for the methanol synthesis (CO_2 reduction) ((iii) in Scheme 2) and the remaining 75-95% for the competing hydrogen evolution reaction ((iv) in Scheme 2).[19]

To our knowledge, the reports from the above two groups,[5,8,10,17-20] which reached very different conclusions, are among the very few experimental studies attempting to elucidate the CO_2-pyridnium mechanism. Other investigators focussed largely on extending the methanol production to different electrode materials[21,22] or on the electrochemistry of pyridine solutions.[23-26] The one closely-related study[27] examined the effect of pyridine on the homogeneous photochemical reduction of CO_2 to methanol using a Ru complex. The main conclusion of this work was the confirmation of methanol synthesis and the important role of pyridine in it, although no specific mechanism was suggested[27].

In view of apparently contradictory reports regarding the catalytic role of pyridine in CO_2 reduction, we have conducted an electrochemical study of the CO_2-pyridinium system under high CO_2 pressures. Using high pressure allows the issue of low solubility of CO_2 in aqueous electrolyte to be overcome, which according to Scheme 2, should help to maximise the proportion of the current going into CO_2 reduction and hence increase the methanol Faradaic yield (FY).

This paper reports the results of bulk electrolysis and cyclic voltammetry studies at high CO_2 pressure for a wide range of pyridine concentrations and a variety of biasing/polarisation conditions, supported by numerical simulations.

Experimental section

High pressure experiments were carried out in a Pyrex container placed inside a water-jacketed stainless steel cell (Parr®) rated to operate up to 350 bars. The pressures were maintained (±0.5 bar) by employing a JASCO BP-2080-81 back pressure regulator. The pressure was applied 1 hour prior to CV measurements or bulk electrolysis to allow CO_2 to saturate the electrolyte. The temperature was stabilised at 20 ± 0.1 °C using a thermostatic water circulator.

Water-based (2-30 ml per charge) electrolyte containing of 0.5 M KCl (Aldrich, >99.9%) with added pyridine (Aldrich, >99.9%) were used. All experiments were performed using a Metrohm Autolab-101 potentiostat. A standard three-electrode arrangement was used with either a Pt wire (areas 0.06 or 0.6 cm²) or foil (3.6 or 10 cm²) as the working electrode, for cyclic voltammetry and bulk electrolysis respectively. Pt mesh (>20 cm², Aldrich, 99.9%) was used as the counter electrode and AgCl-coated Ag wire (Aldrich,

>99.99%) as the (pseudo) reference electrode. Both of these electrodes were placed in separate compartments isolated from the working electrode compartment by fine glass frits and filled with electrolyte identical to that in the working electrode chamber. For experiments under ambient pressure, a standard Ag/AgCl reference electrode (3M KCl) was used. All data in this paper are presented in respect to this reference electrode potential. Prior to experiments, the working Pt electrodes were activated by flaming with a natural gas torch, then soaked in hydrogen peroxide (Fisher Scientific, >30% w/v) followed by concentrated HCl (Aldrich, >99.9%) for 1.5-2 hours each and finally rinsed with deionised water (18 Ωcm^{-1}). Prior to the CO_2 (99.95%) admission, electrolyte solutions were purged for 15-20 min with N_2 (99.94%). In experiments under nitrogen atmosphere, the pH of the solution was adjusted using HCl (Aldrich, >99.9%). All cyclic voltammetry data are presented without the series resistance compensation.

The electrolysis experiments were conducted in a batch manner. After a desired charge (1 - 300 C) had been passed, the high pressure cell was slowly depressurised and the alcohols content of the electrolyte was analysed by GCMS.

The electrolysis products were analysed on an HP6890 gas chromatograph connected to a mass spectrometer (GCMS). Two methods were employed to ensure consistent results. In one method, 1-3 μl of electrolyte solution was injected directly and analysed using an Rt-Q Bond column. In the second method, a headspace analysis was performed using a PLOT-U column. For the latter, the headspace gas was sampled from a vial containing the analysed electrolyte pre-heated to 60°C. In addition to methanol, the levels of isopropanol, ethanol and butanol were monitored. No other products were analysed.

Simulations were conducted with commercial DigiElch software using realistic electrode geometry.

Results and Discussion

CO₂ pressure effect

The CV waves in Py-containing electrolyte taken at different CO_2 pressure indicate a steady increase of the reduction current with CO_2 pressure, as shown in Fig. 1. This is in qualitative agreement with the results reported by the Bocarsly group for the 1-6 bars CO_2 pressure range[7] for similar Py concentrations. The rate of the current increase drops above ~10 bars and approaches saturation above ~50 bars (as can be seen from the experimental data on the inset into Figure 1). Saturation behaviour of this type might be expected in view of the known pressure dependence of CO_2 solubility in water electrolytes. However, if it
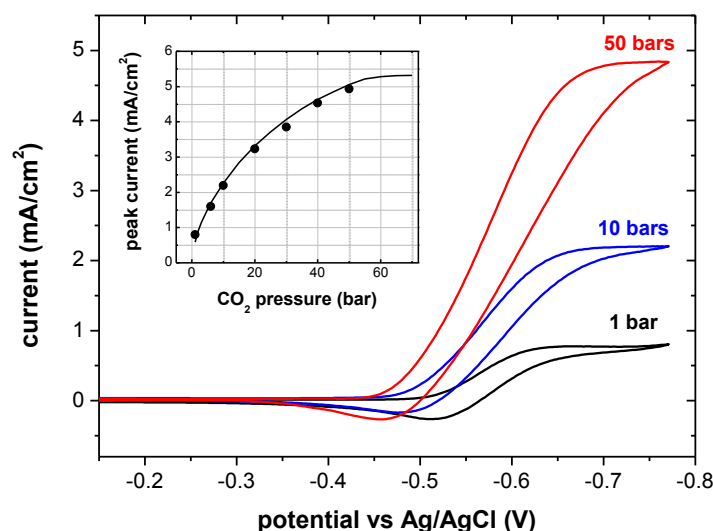

Figure 2. CV waveforms with varying CO_2 pressure: scan speed 10 mV/s, 10 mM of pyridine. Insert: CV reduction peak/limiting current versus CO_2 pressure; symbols – experiment, solid line – simulation.

is due solely to changing solubility, the observed pressure dependence would imply strong deviation from Henry's law and indicate that the dissolved CO_2 concentration increases from 33 mM at 1 bar to 1.27 M at 57 bars (at 20ºC), and changes by less than 5% on the subsequent pressure increase up to 100 bars (Figure S2). On the other hand, in the case of a mechanism involving direct CO_2 participation in the electrode reaction (Scheme 2), the approach to saturation might imply that excess of CO_2 had already been reached. For either scenario, the maximum effect of CO_2 pressure can be expected to be observed already at ~50-60 bars. Hence, the remainder of our experiments were conducted at this pressure range.
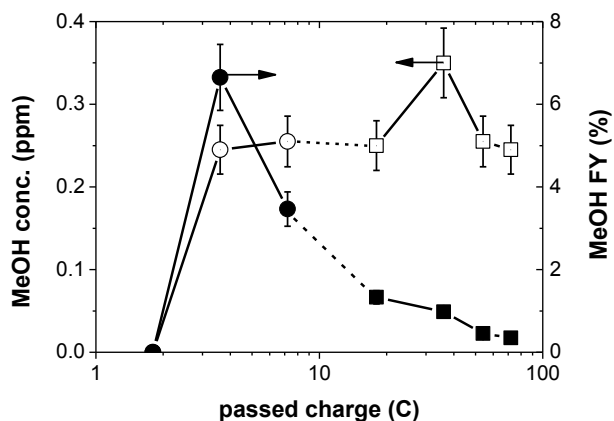

Figure 1. Final methanol concentration and Faradaic yield as function of the passed charge for galvanostatic electrolysis in 50 mM pyridine solution at 55 bars of CO_2 . Current density: circles – 0.05 mA/cm², squares – 0.5 mA/cm². Broken lines added to aid the visual connection between two sets of data only. Error bars reflects the methanol detection accuracy
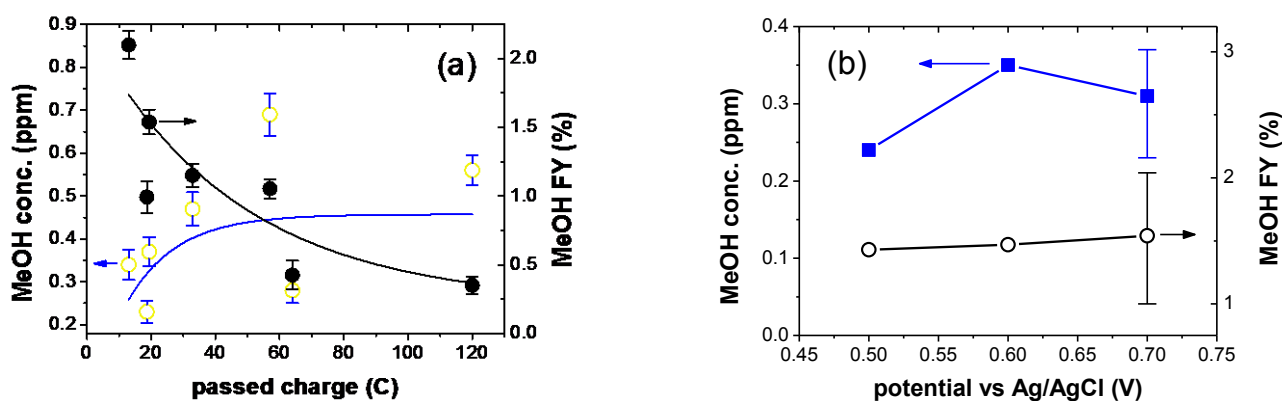
5

Figure 3. Faradaic yield (closed symbols) and final concentration of methanol (open symbols) obtained in potentiostatic bulk electrolysis at 55 bars of CO_2 and 10 mM of pyridine.
(a) As function of the passed charge for the reduction potential of -0.7 V. Error bars reflects the methanol detection accuracy. Solid line are only a guide to the eye.
(b) As function of the reduction potential for the passed charge of 14-19 C. Error bars indicate data scatter over three experiments at -0.7 V. Other data points represent single experimental runs.

In accordance with the CV data, the cathodic potential for bulk electrolysis experiments was chosen to be between -0.5 and -0.8 V (for potentiostatic accumulations). For galvanostatic electrolysis, the cathodic current was fixed at values in the 50 $\mu A/cm^2$ to 1.5 mA/cm^2 range.

Bulk electrolysis

Fig. 2 shows typical variation of the methanol concentration in the electrolyte with passed charge for galvanostatic electrolysis at two different current density values. Methanol was detected after ~1 hour of electrolysis or ~10 C of passed charge, whichever represented the shortest period. At the same time, we were not able to clearly detect the gradual build-up of the methanol concentration with the passed charge. This can be an indication of some latent period in the reduction process. The methanol concentration tends to reach maximal values after 10-20 C of passed charge and remains largely constant thereafter. The latter results in a dynamic character of the apparent Faradaic yield (for methanol production), which starts from ~7% and decays steadily with the accumulated charge (Fig. 2).

An example of the potentiostatic electrolysis (at -0.7 V) can be seen in Fig. 3(a). It shows a similar trend of saturation of the final methanol concentration at sub-ppm level after few tens of coulombs of charge has been passed. Experiments at less negative potentials show no obvious improvement in terms of either the methanol concentration or Faradaic yield. On the other hand, despite all possible measures being taken to ensure consistency, the repeatability of the bulk electrolysis experiments was poor; hence, this could obscure some weak correlations.

A common feature in all electrolysis experiments with these typical Py concentrations is that the final methanol concentration was limited to sub-ppm level irrespective of the charge passed or polarisation mode.

Figure 4 represents the cumulative results of electrolysis performed across a wider range of pyridine concentrations. Each data point shown in Figure 4 corresponds to a passed charge larger than ~10 C so the methanol accumulation has reached or is approaching its limiting value. It can be seen that the final methanol concentration is still no more than ~1 ppm for the entire pyridine concentration range. It should be noted that different pyridine concentration in these experiments results in different equilibrium pH value of the electrolyte, spanning from pH = 3.5 at 1 mM of Py to pH = 5.8 for 1 M of Py. This implies that the hypothetical competition between the hydrogen evolution reaction and CO_2 electro-reduction is shifting with Py concentration. Nevertheless, the data shown in Fig. 4 leads to the conclusion that pyridine concentration is not a critical factor as no clear optimal pyridine concentration or concentration trend is revealed. The apparent FY corresponding to the methanol accumulation shown in Figure 4 is presented
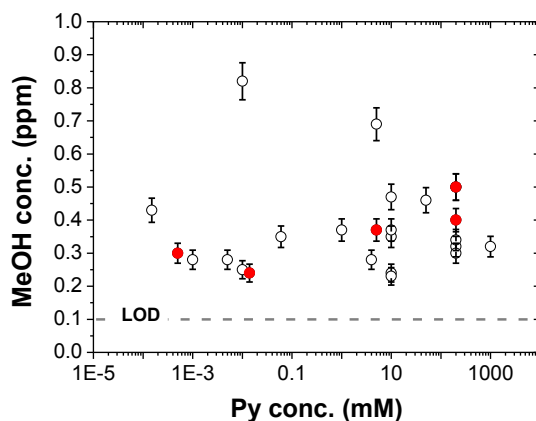
6

Figure 4. Final methanol concentration after electrolysis versus analytical pyridine concentration in electrolyte at 55 bars of CO_2. Passed charge $\geq$ 9 Coulombs for each experiment. Each symbol represents individual experiment: open circles – potentiostatic electrolysis; filled circles – galvanostatic electrolysis. LOD - limit of detection.

in Figure 5. It displays the same dynamics as shown in Figures 2 and 3, starting at ~10% for ~10 C of passed charge and drops steadily with increasing the charge passed. This dynamic behaviour is clearly related to the apparent limit in absolute value of final methanol concentration, which was observed in all our experiments. To the best of our knowledge, a limitation of this nature was not reported by the Bocarsly group or other authors. Neither are we aware of any results contradicting this limited methanol yield and/or the dynamic character of the FY. The observed limit of the methanol yield can explain the failure to detect methanol in the experiments of Costentin et al [15], who were using a less sensitive analytical technique than was employed in the present work.

Interestingly, methanol was obtained at concentrations of pyridine as small as 0.5 μM. The real Py limit could be even lower. Indeed, we have observed the characteristic pyridinium CV waveform in electrolytes with pyridine content below the GCMS detection limit. The latter observation is in agreement with the known high surface activity of pyridine on metals.[28,29] At the same time, the electrolysis (in different polarisation modes) in the high pressure cell, **which has been thoroughly cleaned of pyridine**, did not result in methanol production. Hence we can conclude that it was necessary to have pyridine in the electrolyte in order to obtain methanol in our experiments.

In addition to methanol, comparable concentrations of higher alcohols (ethanol, isopropanol and butanol) were often detected at higher pyridine concentrations (Figure S3). These products have not been reported previously for pyridine-assisted reduction of CO_2 at a Pt (or Pd) electrode. However, the same alcohols were among the products reported[9,10,21-24,30,31] for CO_2 reduction on several semiconductor or composite electrodes in the presence of pyridine or its derivatives (similar nitrogen containing
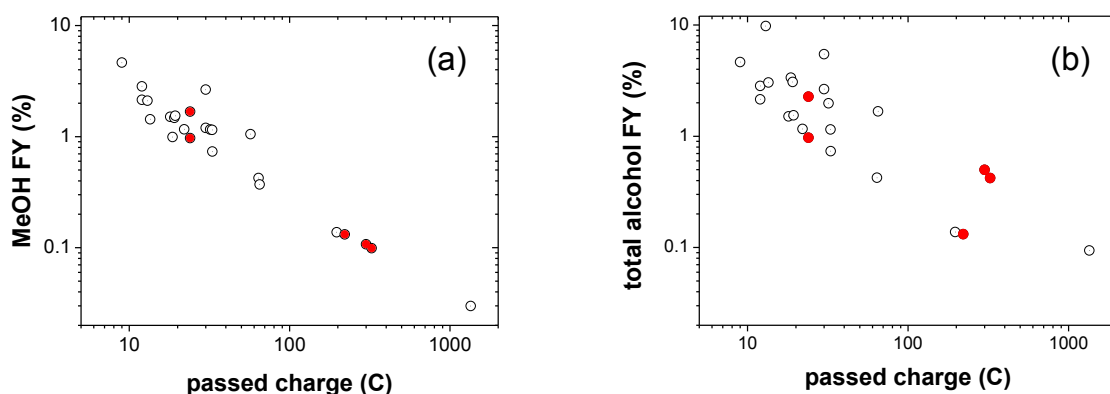

Figure 5. Alcohols Faradaic yields versus passed charge for the bulk electrolysis experiments shown in Fig. 4. (a) methanol FY; (b) total FY including methanol, ethanol, isopropanol and butanol contributions. Each symbol represents individual experiment: open circles – potentiostatic electrolysis; filled circles – galvanostatic electrolysis.

7

heteroaromatic molecules). Inclusion of these alcohols leads to somewhat larger values of the FY but does not change its dynamic character as shown in Figure 5b. The maximal values of this total FY (~10%) are comparable to, but still less than, the 15-20% methanol FY reported for reduction at 1 bar of CO_2 for similar electrodes.[8,17,26] Hence, using a higher concentration of CO_2 does not lead to a higher FY for CO_2 to alcohol reduction. The simultaneous appearance of methanol and higher alcohols is in agreement with the mechanism of multistep reduction of CO_2.[6] In this framework, it would indicate that up-conversion to higher alcohols proceeds more efficiently than further increase of the methanol concentration. This can be interpreted as evidence that the methanol concentration is not limited by the lack of available hydrogen.

Electrode reactivation

The limit to the methanol yield revealed in our experiments casts serious doubt on both the practical applicability of this system for CO_2 reduction and the proposed mechanism[6] for pyridine-assisted CO_2 to methanol reduction. On the other hand, a product limitation is often observed in bulk electrolysis experiments and is usually related to electrode blockage (poisoning) either by products/intermediates or by impurities.[32] A pre-electrolysis step (see experimental details section) designed to remove the cationic impurities from the electrolyte was introduced into preparative electrolysis experiments but failed to increase the methanol yield. Moreover, experiments on repeating the electrolysis (in the same electrolyte) with the re-activated working electrode did not result in increased methanol concentration in the electrolyte either. Both of these experiments imply that blocking of the electrode with impurities is unlikely to be responsible for the limited methanol production.
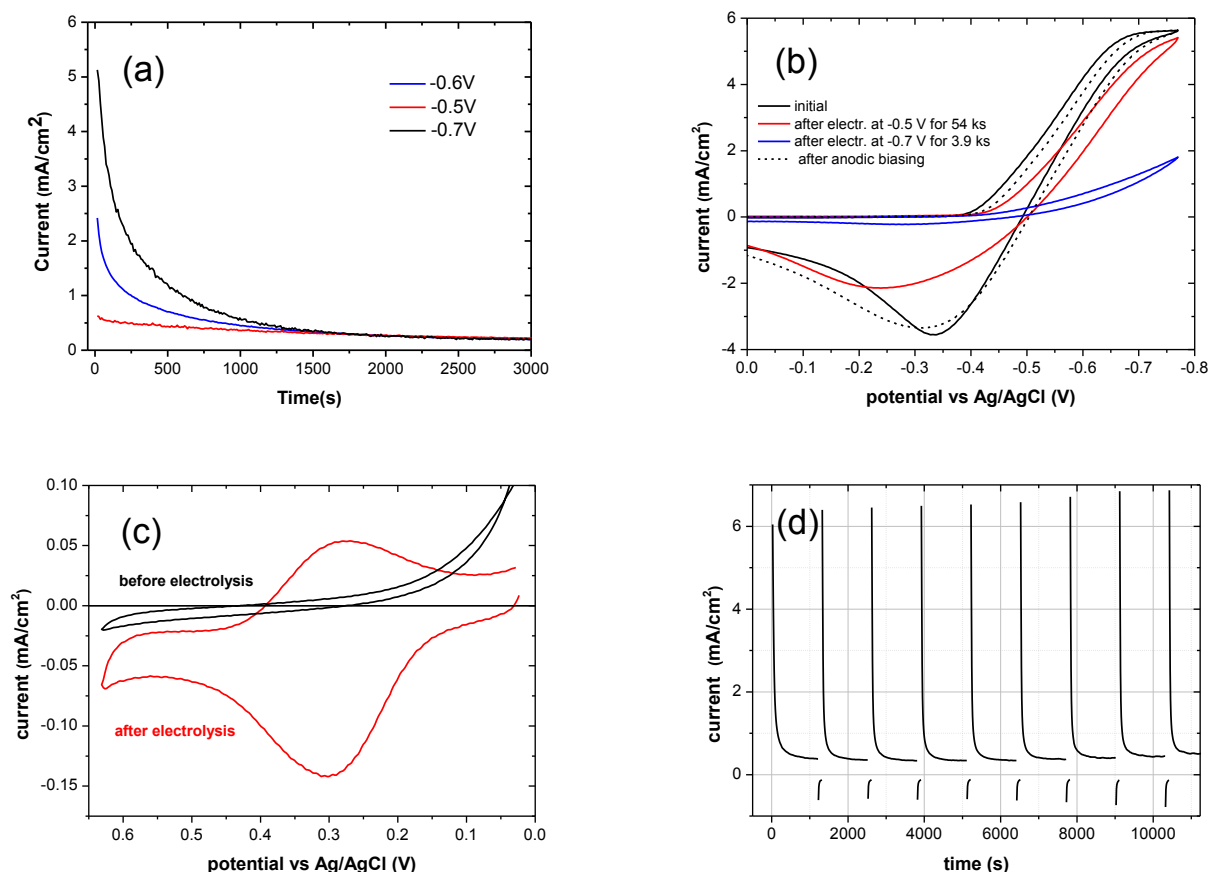

Figure 6. (a) Electrolysis at different fixed potentials, showing current variation with time; (b) CVs before the electrolysis (black curve), after electrolysis at -0.5 V (red curve) and -0.7 V (blue curve); (c) CO desorption wave in the first CV (red curve) taken after the electrolysis at -0.7 V. The first CV taken at the same potential range before the electrolysis is shown (black curve) for comparison; (d) Current variation in bulk electrolysis at electrode potential alternated between -0.7 V and +0.5 V. Scan rate 100 mV/s; 10 mM of Py; 55 bars of CO_2.

Analysis of the time dependence of the electrolysis current nevertheless reveals clear signs of an electrode blockage. Figure 6a shows a typical current variation with time, which displays a quick drop to less than half-value in the first few minutes, eventually stabilising at ~10% of the starting value. The current drop is slower and smaller at less negative polarisation potentials. However, this current drop happens to some extent at all the cathode potentials (in the 0.5-0.8 V range) and it is not sensitive to the introduction of the pre-electrolysis step. Similar electrode blocking was observed (Figure S4) in galvanostatic electrolysis experiments, where it is manifested as a significant negative shift of the cathode potential. The CV wave taken at the blocked electrode displays a distorted shape with a cathodic shift, as demonstrated by Figure 6b, which becomes more severe after electrolysis at more negative potentials (higher current density). In addition, the CV of the blocked electrode also reveals an anodic peak at +0.3 V, as shown in Figure 6c. Electrode polarisation at +0.5 V for a few minutes or several cycles of voltammetry results in disappearance of the anodic peak and restoration of the original CV waveform (Figure 6b) and the electrolysis current. We noted that the revealed anodic wave and its features are very similar to the characteristics[33,34] of the oxidative desorption wave of adsorbed CO molecules (or so-called 'reduced-CO_2' species[34]) on Pt. Considering CO is one of the expected[32] products/intermediates of any CO_2 electro-reduction, and the efficient blocking of Pt electrode by adsorbed CO is a well-known phenomenon, the observed current drop during the electrolysis is most likely happening due to the adsorption of CO molecules on the working electrode. Continued electrolysis after the anodic stripping results in recurrence of the electrode blockage in a somewhat shorter time, which can be explained by quicker poisoning due to CO accumulated in the electrolyte from the preceding electrolysis.

In order to verify the possible connection between the electrode blockage and limited methanol yield, a periodic anodic biasing of the working electrode was incorporated into the preparative electrolysis procedure. Figure 6d displays the current variation with time for potentiostatic electrolysis at -0.7 V with added biasing at +0.5 V for 2 min at every 20 min. The current displayed periodically drops with subsequent recovery resulting in ~5 times increase of the average current. Despite the higher average current value, no statistically significant increase of the methanol yield was observed in these experiments.

Additionally, two other procedures were tested in order to unblock the electrode and improve the methanol yield. One was a contrast electrode polarisation, when the potential of working electrode is switched from -0.9 V to -0 V for 2 min every 30 minutes (see Figure 7a). At the relatively high bias of -0.9 V, gas bubbles (presumably hydrogen) were intensively generated; these are expected to be efficient in replacing the adsorbed CO or preventing the CO adsorption. As a result, a higher average current density was indeed achieved in these experiments, but no improvement of the methanol yield was observed. This result can be explained by the overwhelming competition from the hydrogen generation route due to the high negative potential (-0.9 V) used. Hence, a second activation procedure, suitable for electrolysis at low current density, has been devised.
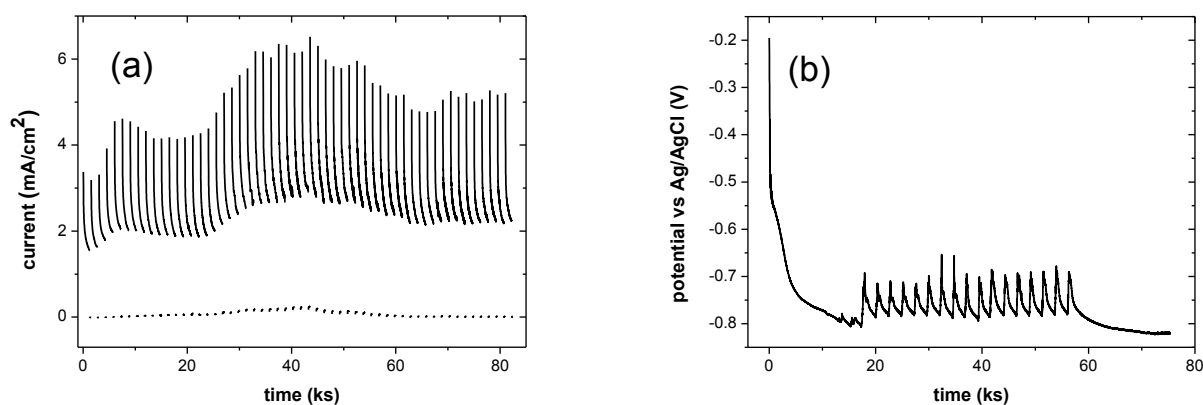

Figure 7. (a) Current variation in bulk electrolysis at electrode potential alternated between -0.9 V and 0 V, 55 bars of CO_2, 200 mM of pyridine (b) Potential variation in galvanostatic electrolysis (-150 $\mu A/cm^2$) at CO_2 pressure alternated between 63 and 20 bars.
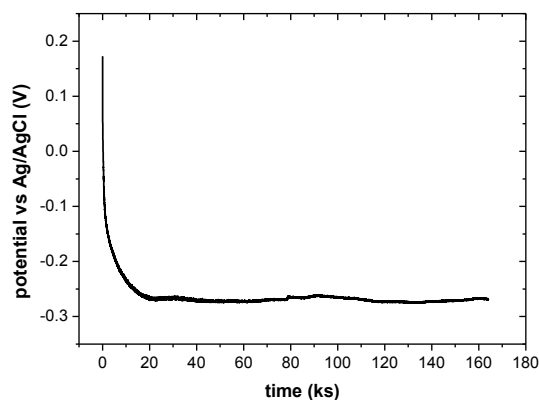
Figure 8. Variation of working electrode potential in galvanostatic electrolysis at -50 µA/cm² for 200 mM of pyridine.

The second procedure was based on periodic variation of the CO_2 pressure inside the reactor. The pressure was first stabilised at 63 bar, then it was quickly dropped to 20 bar and left at this level for 20 minutes. After that, the pressure was raised back to 63 bar and preserved for another 20 minutes. This pressure cycling was repeated for ca. 10 hours with the cathode current held at 150 µA/cm². The idea for the pressure cycling was to produce massive adsorption of excess CO_2 molecules on the electrode surface, after this excess has been induced in the electrolyte by the sudden pressure drop. The adsorbed CO_2 molecules are expected to be gathered in micro-bubbles and subsequently in macro-bubbles (confirmed visually), presumably replacing the adsorbed CO molecules. This procedure also failed to increase the methanol yield, although it helped to keep the electrode potential positive of -0.8 V (see Figure 7b).

The overall outcome of all three series of experiments with different techniques for reactivation of the working electrode implies that the observed blocking of the electrode is unlikely be directly responsible for the observed limit for methanol production. Hence, the reason for the latter remains unclear. At the same time, the apparent insensitivity of methanol production to the electrode current density and polarisation potential can be interpreted as evidence of decoupling of methanol production from charge transfer on the electrode. This idea is further supported by the observation of methanol production during electrolysis at under-potential conditions, which was reported in galvanostatic experiments at low current density and high Py concentration. The variation of the electrode potential for one such experiment is shown in Figure 8. For the entire duration of electrolysis, the potential did not exceed -0.3 V, which is significantly less negative than equilibrium potentials of HER (-0.57 V) and CO_2 to MeOH reduction (-0.54 V) at similar acidity (pH = 5.46). On the other hand, the -0.3 V potential is sitting well into the region of the hydrogen adsorption pre-peak normally observed on CVs of pyridinium at high scan rates (Figure 9, discussed later). This implies that adsorbed hydrogen was the only electrode reduction product and the CO_2 reduction follows afterwards via reaction with this hydrogen.

The degree of coupling of the CO_2 reduction to the electrode processes can be further judged from the CV analysis via Nicholson criteria and numerical simulation, which are described below.

Cyclic voltammetry

As a first step in the simulation, a set of apparent reaction parameters was obtained from fitting of the experimental CV waveforms obtained in pyridinium acidic solution under an inert atmosphere. Initially, the reaction Scheme 1 was tested. It was found that the simulated reduction peak current significantly underestimated the experimental values (by ~30%) for higher scan speeds and Py concentrations. This peak current limit is set by the fundamental upper limit of the deprotonation rate constant of pyridinium. The latter is defined by the product of the well-known K_A value and the fastest possible protonation rate (estimated at ~10^{10} s⁻¹M⁻¹). Hence, an alternative or parallel electrode reduction process has to be considered in order to reproduce the experimental values. Accordingly, reduction of PyH ions through
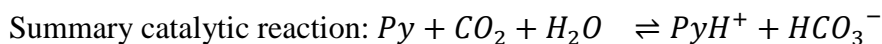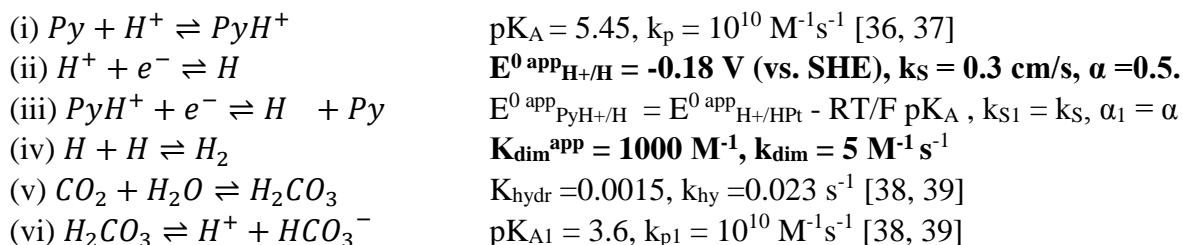
proton coupled electron transfer (PCET) was added to the simulation as a second electrode reaction (reaction (ii) in Scheme 2). The redox potentials for these two electrode reactions are not independent. Assuming fast PyH$^+$ <=> Py + H$^+$ equilibrium, E$^{0\ app}$$_{PyH+/HPt}$ = E$^{0\ app}$$_{H+/HPt}$ - RT/F pK$_A$. The individual contribution of each of the two reduction routes depends on Py content and pH. Our simulations indicate that for not very acidic conditions the PCET route dominates the current. This is in agreement with detailed polarographic studies of pyridine.[35] The final reaction system used for the simulation is shown in Scheme 3. In this scheme, the dimerization (reaction (iv)) has been taken as main conversion route of adsorbed hydrogen into molecules. In reality, the dimerization is a surface reaction, whereas all present simulations were conducted with freely diffusing atomic hydrogen. Hence all simulation parameters for the freely diffusing hydrogen atoms are totally fictitious but serve the purpose of imitating the process of hydrogen accumulation and transport away from the electrode [*]. For the present discussion it is important that the fictitious bulk dimerization reaction has a negligible effect on the simulated cathodic peak current, while affecting the overall CV shape via the anodic peak.

Reaction Scheme 3 (first four reactions) has been used to fit the experimental CV data for 10 mM Py in 0.5 M KCl electrolyte, obtained at pH =5.5 (HCl adjusted) in nitrogen-purged solution at atmospheric pressure. The fitting results are presented in Fig. 9, which demonstrates good agreement between the simulated and experimental waveforms for a wide range of scan speeds. A significant deviation is observed only for the enhanced current background in the potential range of 0.25-0.45 V. This enhanced background (or foot current) has been observed before in cyclic voltammograms of weak acids on Pt and was associated with the hydrogen adsorption pre-wave.[40] This interpretation is in agreement with our reaction scheme and further supported by the observed variations of this pre-wave current with the scan speed and Py concentration (Figure S5).

The set of fitting parameters (E$^{0\ app}$$_{H+/H}$, k$_S$, α, K$_{dim}$^{app} , k$_{dim}$) obtained from this fitting was directly applied to simulate the CV waveforms for other Py concentrations (from 5-200 mM range) in similar pH-adjusted nitrogen-purged solutions. Reasonably good agreement between the simulated and experimental waveforms was obtained. For the cathodic peak current in particular, the simulated values do not deviate from the experimental ones by more than 15% (compared to ~10% experimental reproducibility) for a wide range of the scan speed, as shown in Fig. 10a. It was also found from the simulation that the current contribution from the direct proton reduction route (reaction (ii) in Scheme 3) is negligible compared to the pyridinium PCET (reaction (iii) in Scheme 3) for the entire range of pyridine concentrations at pH = 5.5.

Finally, the same set of model parameters was applied to simulate the CV data obtained at high CO$_2$ pressure. It was found that the main features of the experimental CV waves were reasonably well reproduced as demonstrated in Figure 11. Here again, the agreement between the simulated and

---

Scheme 3. Set of reactions used in the simulation of experimental data at 20°C. Fitting parameters are in bold.

(i) $Py + H^+ \rightleftharpoons PyH^+$ pK$_A$ = 5.45, k$_p$ = 10^{10} M^{-1}s^{-1} [36, 37]

(ii) $H^+ + e^- \rightleftharpoons H$ **E$^{0\ app}$$_{H+/H}$ = -0.18 V (vs. SHE), k$_S$ = 0.3 cm/s, α =0.5.**

(iii) $PyH^+ + e^- \rightleftharpoons H\ \ + Py$ E$^{0\ app}$$_{PyH+/H}$ = E$^{0\ app}$$_{H+/HPt}$ - RT/F pK$_A$, k$_{S1}$ = k$_S$, α_1 = α

(iv) $H + H \rightleftharpoons H_2$ **K$_{dim}$^{app} = 1000 M^{-1}, k$_{dim}$ = 5 M^{-1} s^{-1}**

(v) $CO_2 + H_2O \rightleftharpoons H_2CO_3$ K$_{hydr}$ =0.0015, k$_{hy}$ =0.023 s^{-1} [38, 39]

(vi) $H_2CO_3 \rightleftharpoons H^+ + HCO_3^-$ pK$_{A1}$ = 3.6, k$_{p1}$ = 10^{10} M^{-1}s^{-1} [38, 39]

Summary catalytic reaction: $Py + CO_2 + H_2O\ \ \rightleftharpoons PyH^+ + HCO_3^-$

Diffusion coefficients (10^{-5} cm^2 s^{-1}): D$_{H+}$ = 10, D$_H$ = D$_{H2}$ = 5, D$_{Py}$ = 0.6, D$_{PyH+}$ = 1, D$_{CO2}$ = 1.5, D$_{H2CO3}$ = D$_{HCO3-}$ = 1.2 [15].
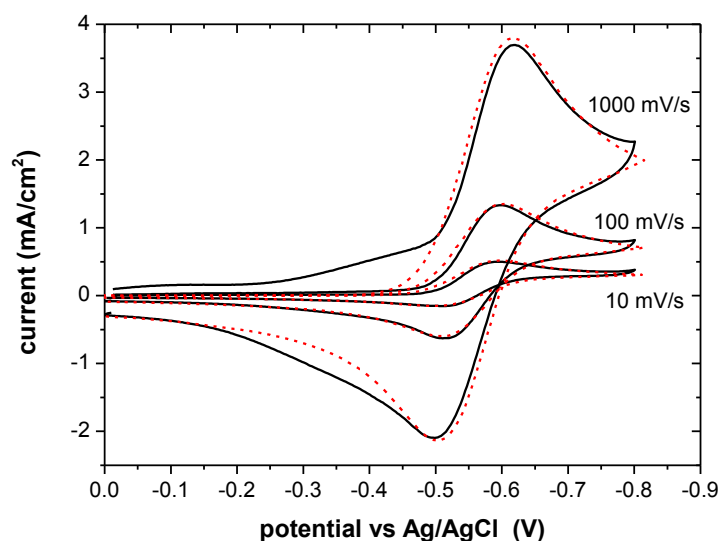
Figure 10. CV of 10 mM Py at pH = 5.5 for 10, 100 and 1000 mV/s scan speed. Black solid lines - experiment, red dashed lines – simulation.

experimental values of the cathodic peak current is better than 10-15% for the scan speed in 10-5000 mV/s range, as shown in Fig. 10b.

In accordance with Scheme 3, the effect of CO_2 on the electrode reactions can be classified as a preceding chemical reaction (CE type) supplying protons for the first electrode reaction (ii), and as a subsequent catalytic re-protonation of pyridine (EC' process) for the second electrode reaction (iii). Considering the negligible contribution of the first electrode reaction for the Py concentration range under consideration (10-200 mM), the CV shapes in presence of CO_2 should reflect the EC' process [**]. Analysis of Fig. 11 indicates that the CV voltammograms under high CO_2 pressure display features characteristic of the coupled catalytic chemical reaction (EC'). This can be further illustrated using established Nicholson diagnostic criteria. First we note that taking into account a significant excess of dissolved CO_2, the summary catalytic reaction can be treated as a pseudo-first order one. Hence, the Nicholson diagnostic is indeed applicable at least on a qualitative level. Next, from the comparison of Fig. 10a and 10b, one can immediately notice a significant (several times) increase of the reduction peak current under CO_2. This demonstrates that the kinetic current component is much larger than the diffusion one, i.e. this EC' case is well-pronounced. In addition, from the analysis of Fig. 10b, one can see that the reduction peak current becomes insensitive to the scan speed at lower scan speeds, approaching a limiting
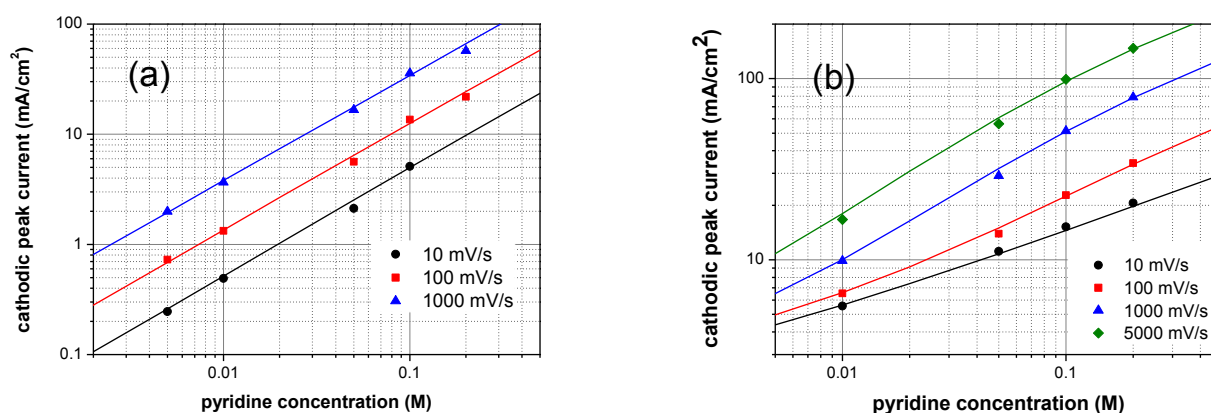

Figure 9. (a) CV cathodic peak current at different Py concentrations at pH = 5.5 in inert atmosphere at 1 bar: symbols - experiment, lines - simulation. (b) Cathodic peak current as a function of pyridine total concentration for CVs at 55 bars CO_2: symbols - experiment, lines - simulation.
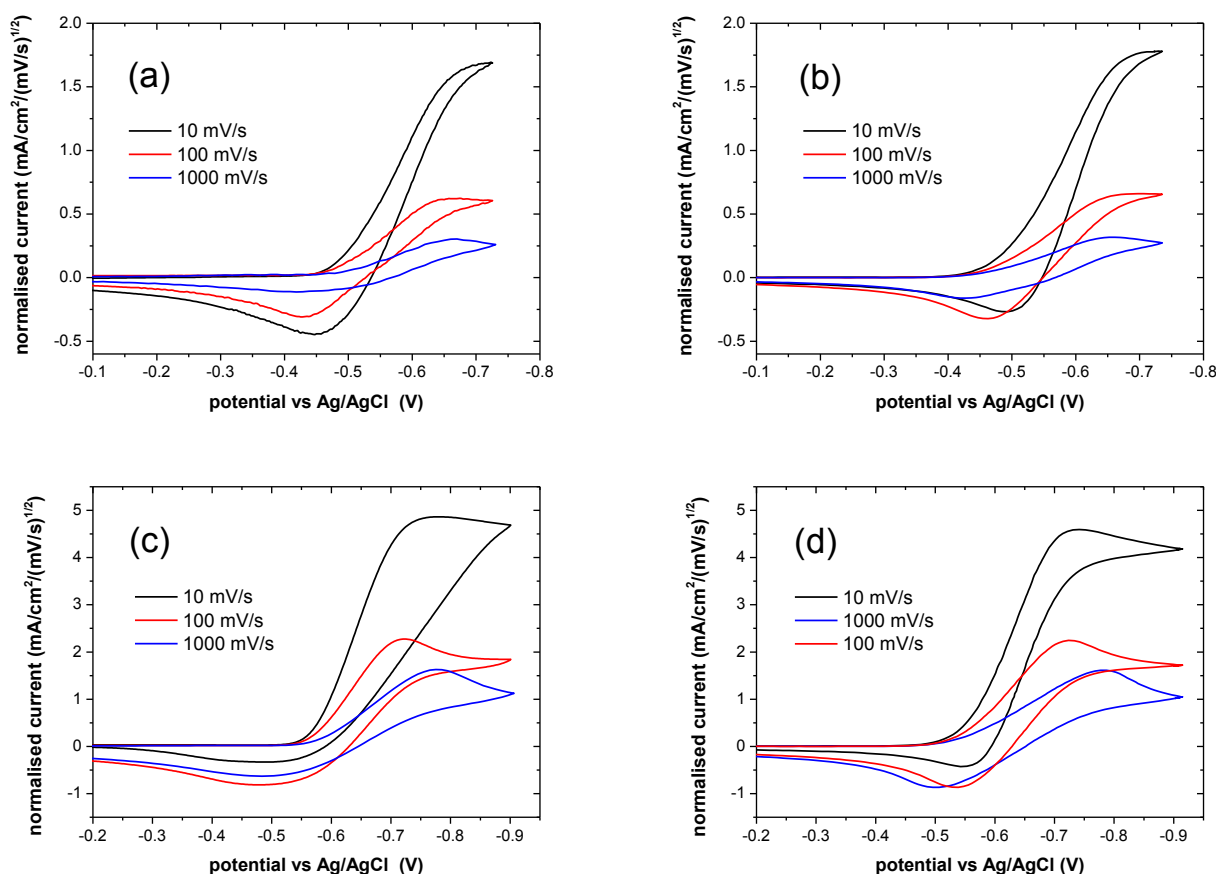
Figure 11. CV for 10 mM Py (top row) and 100 mM Py (bottom row) for different scan rates at 55 bars of CO_2. Left images - experiment, right - simulation.

value. This effect is most pronounced for the lower pyridine concentration, when the re-protonation is more efficient for a given CO_2 concentration. The same limiting current behaviour is also responsible for the S-shape of the CV waveform at low scan speed (see Fig. 11). In agreement with Nicholson and Shain [41], these characteristic features indicate that the current is dominated by a kinetic component which is proportional to the re-protonation rate of pyridine via the coupled chemical reaction in EC' scheme.

The simulation can also reproduce the variation of the CV peak current with CO_2 pressure, shown in the insert to Fig. 1. According to the simulation data, the initial sharp rise of the current reflects the joint effect of increasing PyH^+ concentration and growing kinetic current component. At ~30 bar pressure, 99% of 10 mM pyridine is already protonated and also the concentration of aqueous CO_2 has started to deviate from Henry's law (Figure S2). Hence, the total reduction current begins to approach saturation at > 30 bars. The reasonable agreement between the simulation and experiment allows us to conclude that the rise of the reduction current in the presence of CO_2 cannot be taken as evidence of CO_2 reduction.

To summarise, the CV analysis suggests that the experimental data can be well explained within reaction Scheme 3, without any extra (rate-affecting) reaction path needing to be invoked. In other words, within the accuracy of this analysis, there is no evidence for any CO_2 electro- or chemical reduction process in our experimental CV data. The consequences for mechanism Scheme 2 are that reaction (iii) is not prominent, with any contribution being below our simulation accuracy (~10%). Moreover, this conclusion contradicts the expectations of Scheme 2, which predicts that the contribution from reaction (iii) will increase significantly above the stated 5-20% at elevated CO_2 pressure. On the other hand, this conclusion from the CV analysis is compatible with the bulk electrolysis results discussed earlier, which revealed some sort of threshold-like transient CO_2 reduction consuming a maximum of ~10% of the passed charge.

Conclusions

Our electrolysis experiments have confirmed the possibility of CO_2 reduction into methanol on a platinum electrode in the presence of pyridine, as well as the necessity of pyridine for this process. Although the higher CO_2 pressure results in higher cathodic current (for fixed Py concentration), it does not lead to the higher FY for CO_2 to methanol reduction. In addition to methanol, we have also observed the appearance of higher alcohols among the electrolysis products for large concentrations of pyridine in the electrolyte. At the same time, our results revealed the limitation of the reduction process, which was not reported before. Specifically, we found that the final methanol concentration obtained by preparative electrolysis is limited to the ~1 ppm level irrespective of the amount of passed charge or of the pyridine concentration. Importantly, the methanol concentration failed to increase with electrode reactivation.

The CV analysis of pyridine-containing electrolytes indicated that hydrogen evolution is still the dominating electrode reaction even at high CO_2 pressure. Within the analysis accuracy, there is no observable contribution from either a direct or coupled CO_2 reduction.

Altogether, these results suggest that the observed methanol is the result of a chemical reaction between pre-generated hydrogen and CO_2, mediated by pyridine/pyridinium molecules. The underpotential reduction points to the important role of adsorbed hydrogen and platinum surface in this methanol production, which is in agreement with the proposed mechanism [13, 17 and 18]. But in contrast to the predictions of the latter, the methanol production has limited character that can be explained as being a result of very narrow favourable 'window' of experimental parameters which realised only as a relatively short-living transient state during the preparative electrolysis. One of these parameters is likely to be a composition of species (H, Py, CO) adsorbing on platinum surface in a competitive manner. An example of such 'transient' reduction process was reported for the case of copper ion-assisted CO reduction to methanol on platinum.[42]

In terms of the prospective practical value of CO_2 reduction in a pyridine-containing electrolyte, the observed limitation of the methanol accumulation level appears as the most significant obstacle. Further mechanistic studies are needed to understand this effect.

Footnotes

* Here it should be noted that even conducting a true surface simulation still does not provide an adequate model for the real process. Indeed, for the Py concentrations and pH values involved in these experiments, the electrode reduction result in near-electrode accumulation of molecular hydrogen exceeding the hydrogen solubility limit by orders of magnitude. In reality, this excess is taken away via generation of gas bubbles. This nontrivial process would also have to be included in any realistic simulation.

** At low Py concentration, when the proton concentration becomes larger or comparable to that of the pyridinium ions, the experimental CVs indeed display CE features (Figure S5), as expected from the Scheme 3.

References

1. B.Metz, O. Davidson, H. C. de Coninck, M. Loos, and L. A. Meyer (eds.). IPCC Special Report on Carbon Dioxide Capture and Storage, 2005. Prepared by Working Group III of the Intergovernmental Panel on Climate Change, Cambridge University Press, Cambridge, U.K. and New York, USA

2. H. Li & C. Oloman, The Electro-Reduction of Carbon Dioxide in a Continuous Reactor. *J. Appl. Electrochem.*, 2005, **35,** 955–965.

3. H. Li & C. Oloman, Development of a Continuous Reactor for the Electro-Reduction of Carbon Dioxide to Formate - Part 1: Process variables. *J. Appl. Electrochem.,* 2006, **36,** 1105–1115.

4. H. Li & C. Oloman, Development of a Continuous Reactor for the Electro-Reduction of Carbon Dioxide to Formate - Part 2: Scale-up. *J. Appl. Electrochem.,* 2007, **37,** 1107–1117.

5. E. E. Barton, D. M. Rampulla, A. B. Bocarsly, Selective Solar-Driven Reduction of CO_2 to Methanol Using a Catalyzed p-GaP Based Photoelectrochemical Cell. *J. Am. Chem. Soc.,* 2008, **130,** 6342–6344.

6. E. B. Cole *et al.* Using a One-Electron Shuttle for the Multielectron Reduction of CO_2 to Methanol: Kinetic, Mechanistic, and Structural Insights. *J. Am. Chem. Soc.,* 2010, **132,** 11539–11551.

7. A. J. Morris, R. T. McGibbon, A. B. Bocarsly, Electrocatalytic Carbon Dioxide Activation: The Rate-Determining Step of Pyridinium-Catalyzed CO_2 Reduction. *ChemSusChem.,* 2011, **4,** 191–196.

8. G. Seshadri, C. Lin, A. B. Bocarsly, A New Homogeneous Electrocatalyst for the Reduction of Carbon Dioxide to Methanol at Low Overpotential. *Journal of Electroanalytical Chemistry*, 1994, **372,** 145–150.

9. N. R. de Tacconi *et al.,* Electrocatalytic Reduction of Carbon Dioxide Using Pt/C-TiO_2 Nanocomposite Cathode. *Electrochem. Solid-State Lett.*, 2012, **15,** B5.

10. A. B. Bocarsly *et al.,* Comparative Study of Imidazole and Pyridine Catalyzed Reduction of Carbon Dioxide at Illuminated Iron Pyrite Electrodes. *ACS Catal.,* 2012, **2,** 1684–1692.

11. J. A. Keith & A. A. Carter, Electrochemical Reactivities of Pyridinium in Solution: Consequences for CO_2 Reduction Mechanisms. *Chem. Sci.,* 2013, **4,** 1490–1496.

12. J. A. Tossell, Calculation of the Properties of Molecules in the Pyridine Catalyst System for the Photochemical Conversion of CO_2 to Methanol. *Comput. Theor. Chem.,* 2011, **977,** 123–127.

13. M. Z. Ertem, S. J. Konezny, C. M. Araujo, V. S. Batista. Functional Role of Pyridinium during Aqueous Electrochemical Reduction of CO2 on Pt(111). *J. Phys. Chem. Lett.,* 2013, **4,** 745-448.

14. C. H. Lim, A. M. Holder & C. B. Musgrave. Mechanism of Homogeneous Reduction of CO_2 by Pyridine: Proton Relay in Aqueous Solvent and Aromatic Stabilization. *J. Am. Chem. Soc.,* 2013, **135,** 142–54.

15. C. Costentin, J. C. Canales, B. Haddou & J.-M. Savéant. Electrochemistry of Acids on Platinum. Application to the Reduction of Carbon Dioxide in the Presence of Pyridinium Ion in Water. *J. Am. Chem. Soc.,* 2013, **135,** 17671–17674.

16. Y. Yan, E. L. Zeitler, J. Gu, Y. Hu & A. B. Bocarsly. Electrochemistry of Aqueous Pyridinium: Exploration of a Key Aspect of Electrocatalytic Reduction of CO_2 to Methanol. *J. Am. Chem. Soc.,* 2013, **135,** 14020–14023.

17. K. Liao, M. Askerka, E. L. Zeitler, A. B. Bocarsly, V. S. Batista. Electrochemical Reduction of Aqueous Imidazolium on Pt(111) by Proton Coupled Electron Transfer. *Top. Catal*., 2015, **58**, 23-29.

18. E. L. Zeitler, M. Z. Ertem, J. E. Pander III, Y. Yan, V. S. Batista, A. B. Bocarsly. Isotopic Probe Illuminates the Role of the Electrode Surface in Proton Coupled Hydride Transfer Electrochemical Reduction of Pyridinium on Pt(111). *J. Electrochem. Soc.,* 2015, **162**, H938-H944.

19. E. E. Barton Cole *et al.* Substituent Effects in the Pyridinium Catalyzed Reduction of CO_2 to Methanol: Further Mechanistic Insights. *Top. Catal.,* 2015, **58,** 15–22.

20. J. Keith & E. Carter. Theoretical Insights Into Pyridinium-Based Photoelectrocatalytic Reduction of CO_2. *J. Am. Chem. Soc.,* 2012, **134,** 7580–7583.

21. G. Zeng, J. Qiu, Z. Li, P. Pavaskar & S. B. Cronin. CO_2 Reduction to Methanol on TiO 2 -Passivated GaP Photocatalysts. *ACS Catal.,* 2014, **4,** 3512–3516.

22. J. Yuan, L. Zheng & C. Hao. Role of Pyridine in Photoelectrochemical Reduction of CO_2 to Methanol at a CuInS2 Thin Film Electrode. *RSC Adv.,* 2014, **4,** 39435.

23. A. J. Lucio & S. K. Shaw. Pyridine and Pyridinium Electrochemistry on Polycrystalline Gold Electrodes and Implications for CO_2 Reduction. *J. Phys. Chem. C,* 2015, **119,** 12523–12530.

24. H.-P. Yang, S. Qin, H. Wang & J.-X. Lu. Organically Doped Palladium: a Highly Efficient Catalyst for Electroreduction of CO_2 to Methanol. *Green Chem.,* 2015, 5144–5148.

25. E. Lebègue, J. Agullo, M. Morin, D. Bélanger. The Role of Surface Hydrogen Atoms in the Electrochemical Reduction of Pyridine and CO2 in Aqueous Electrolyte. *ChemElectroChem, 2014,* **1**, 1013-1016.

26. E. Portenkirchner *et al.* A Comparison of Pyridazine and Pyridine as Electrocatalysts for the Reduction of Carbon Dioxide to Methanol. *ChemElectroChem,* 2014, **1**, 1543-1548.

27. D. J. Boston, C. Xu, D. W. Armstrong & F. M. MacDonnell. Photochemical Reduction of Carbon Dioxide to Methanol and Formate in a Homogeneous System with Pyridinium Catalysts. *J. Am. Chem. Soc.,* 2013, **135,** 16252–16255.

28. C. Shannon, D. G. Frank, A. T. Hubbard. Electrode reactions of well-characterised adsorbed molecules. *Annu. Rev. Phys. Chem.,* 1991, **42**, 393-431.

29. E. K. Krauskopf, L. M. Rice-Jackson, A. Wieckowski. Pyridine adsorption on polycrystalline platinum studied by the radioactive-labeling method. *Langmuir,* 1990, **6**, 970-973.

30. A. B. Bocarsly. Conversion of CO_2 to Organic Products. *Pat. Appl. Publ.,* 2013, **1,** 1–10.

31. K. Keets, A. Morris, E. Zeitler, P. Lakkaraju, A. Bocarsly. Catalytic conversion of carbon dioxide to methanol and higher order alcohols at a photoelectrochemical interface. *Proc. SPIE Solar Hydrogen and Nanotechnology,* 2010, **7770,** 77700R.

32. Y. Hori. Electrochemical CO_2 Reduction on Metal Electrodes. *Modern Aspects of Electrochemistry,* 2008, **42,** 89–189.

33. A. Rodes, E. Pastor, T. Iwasita. Structural effects on CO_2 reduction at Pt single-crystal electrodes. *J. Electroanal. Chem.*, 1994, **377**, 215-225.

34. M. Lukaszewski, H. Siwek, A. Czerwinski. Electrosorption of carbon dioxide on platinum group metals and alloys – a review. *J. Solid State Electrochem.*, 2009, **13**, 813-827.

35. S. G. Mairanovskii, *Catalytic and kinetic waves in polarography*, Plenum Press, New York, 1968.

36. S. G. Mairanovskii, L. I. Lishcheta. Rate constants of pyridine protonation at variouse temperatures as found from polarographic catalytic hydrogen waves. *Bulletin of the Academy of Sciences of the USSR, Division of chemical science*, 1962, **11**, 209-216.

37. M. K. Poluektov, S. G. Mairanovskii. Influence of the concentration and nature of the cation of indifferent electrolytes on the polarographic catalytic waves of hydrogen induced by pyridine in unbuffered solutions. *Bulletin of the Academy of Sciences of the USSR, Division of chemical science*, 1965, **14**, 400-405.

38. K. G. Schulz *et al*. Determination of the rate constants for the carbon dioxide to bicarbonate inter-conversion in pH-buffered seawater systems. *Marine Chemistry,* 2006, **100,** 53-65.

39. X. Wang *et al*. Comprehensive Study of the Hydration and Dehydration Reactions of Carbon Dioxide in Aqueous Solution. *J. Phys. Chem. A,* 2010, **114**, 1734-1740.

40. S. E. Treimer, D. H. Evans. Electrochemical reduction of acids in dimethyl sulfoxide. CE mechanisms and beyond. *J. Electroanal. Chem.*, 1998, **449**, 39-48.

41. R. S. Nicholson & I. Shain. Theory of Stationary Electrode Polarography. *Anal. Chem.*, 1964, *36* (4), 706–723.

42. B. I. Podlovchenko, T. D. Gladysheva. Copper ion-catalysed electrochemical synthesis of methanol from carbon monoxide on palladium electrodes. *Mendeleev Commun.*, 2006, **16**(4) 232-233.

Table S1. Calculated concentrations of species in 10 mM pyridine 0.5 M KCL solution saturated with CO_2 at different pressure (1-55bars) and 20^oC.

| Pressure (bars)	CO_2 (M)	pH	HCO_3^- (mM)	PyH^+ (mM)	Py (mM)
1	0.0339	5.50	4.73	4.73	5.27
6	0.2016	4.93	7.68	7.67	2.32
10	0.3286	4.75	8.33	8.32	1.68
45	1.145	4.27	9.44	9.38	0.62
50	1.218	4.24	9.47	9.42	0.58
55	1.281	4.22	9.50	9.44	0.56
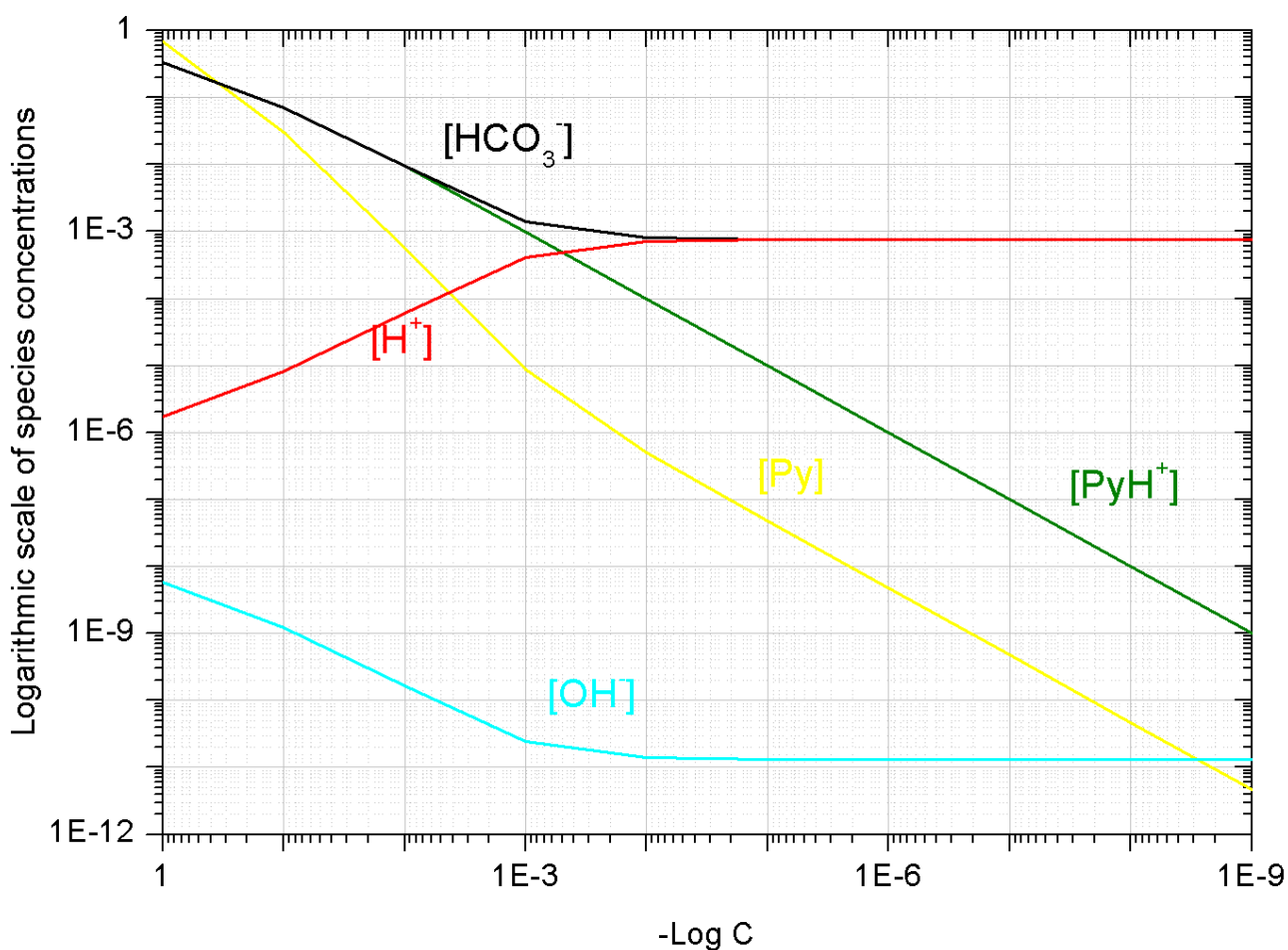
Figure S1. Calculated concentrations of species as a function of analytical concentration of pyridine at 55 bars of CO_2 and 20^oC.
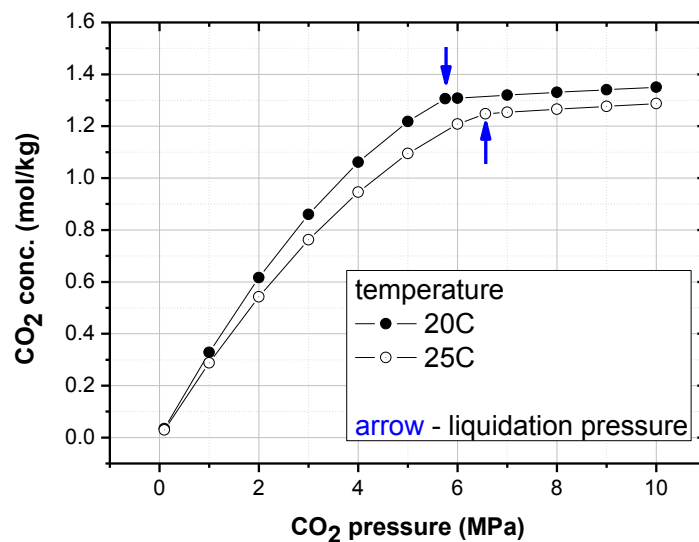
Figure S2. Variation of dissolved CO_2 concentration as function of CO_2 pressure in 0.5 M KCl water solution. Arrows indicate gas-liquid transition pressure.
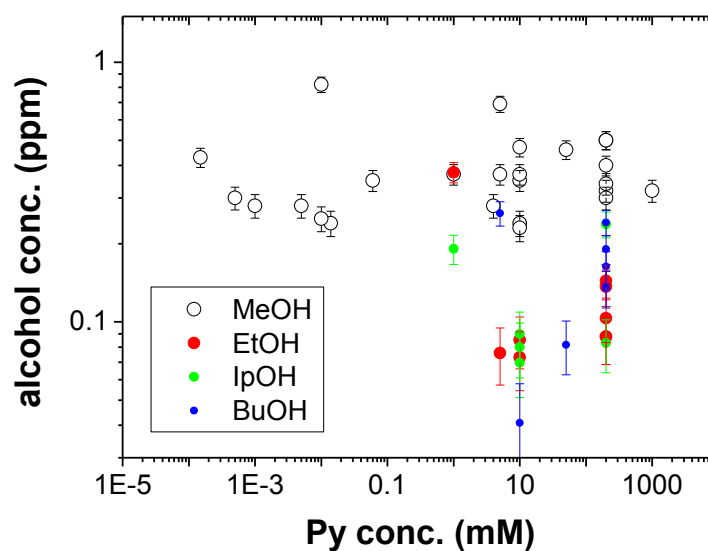
Figure S3. In addition to methanol, comparable concentrations of ethanol, isopropanol and butanol were often detected at higher pyridine concentrations in bulk electrolysis at 55 bars of CO_2.
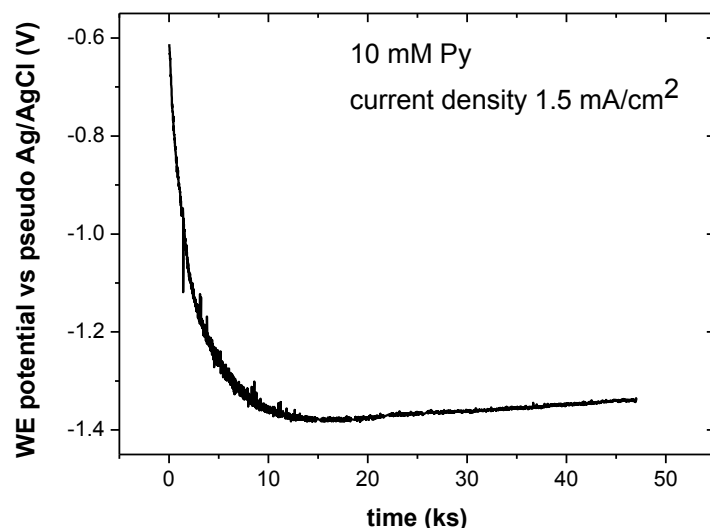
Figure S4. The cathode potential drift during the galvanostatic electrolysis, manifesting a significant negative shift as a result of the electrode blocking.
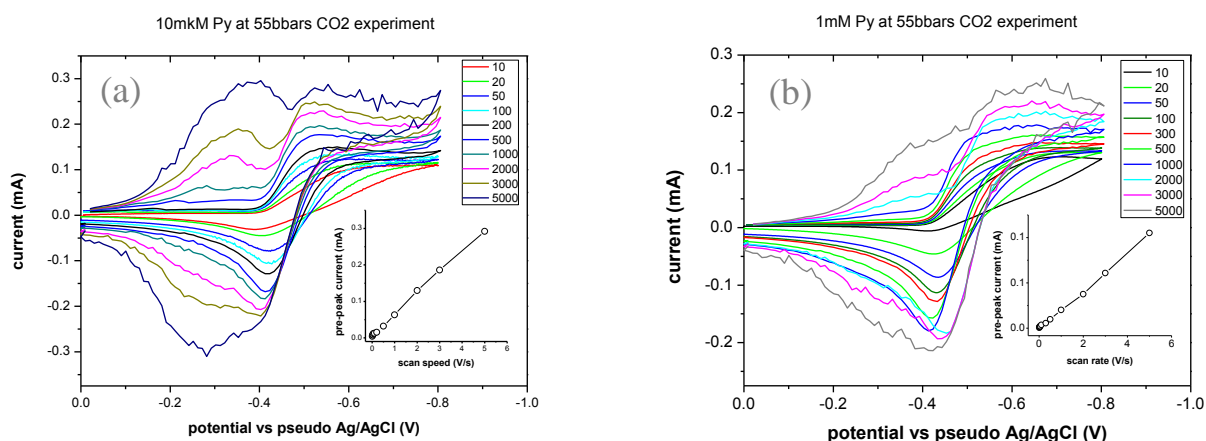
Figure S5. CVs at (a) 1 mM and (b) 10 μmole of pyridine under CO_2 (55 bars) showing the pre-wave at 0.25-0.45V. Insert shows the pre-wave amplitude vs scan rate. The pre-wave grows faster than the main peak, displaying a linear increase with the scan rate. The pre-wave is more pronounced at low pyridine concentration in agreement with earlier observations [S. E. Treimer, D. H. Evans. Electrochemical reduction of acids in dimethyl sulfoxide. CE mechanisms and beyond. *J. Electroanal. Chem*., 1998, **449**, 39-48].